Journal of Luminescence 275 (2024) 120785

Contents lists available at ScienceDirect

Journal of Luminescence

journal homepage: www.elsevier.com/locate/jlumin

Full Length Article

High luminous efficiency and Ultra-Stable $CsPbBr_3$@$CsPb_2Br_5$:Sr core-shell microplate for white light emitting diodes

Chen Zhang [a], Minqiang Wang [a,*], Zheyuan Da [a], Jindou Shi [a], Junnan Wang [a], Qing Yao [a], Nikolai V. Gaponenko [b]

[a] Electronic Materials Research Laboratory, Key Laboratory of the Ministry of Education International Center for Dielectric Research&Shannxi Engineering Research Center of Advanced Energy Materials and Devices, Xi'an Jiaotong University, 710049, Xi'an, China
[b] Belarusian State University of Informatics and Radioelectronics, P. Browki 6, 220013, Minsk, Belarus

ARTICLE INFO

Keywords:
Perovskite
Quantum dots
$CsPb_2Br_5$
Sr-doped
White light emitting diodes

ABSTRACT

$CsPbX_3$ (X = Br, Cl, and I) perovskite quantum dots (QDs) have become promising materials for phosphors and solar cells due to their remarkable photovoltaic properties. However, the high defect density and sensitivity to the surrounding environment have hindered the commercial application of the materials in the field of optoelectronics. Core-shell structures have been proved to be an effective method for passivating surface defects and improving stability. However, the complex post-processing tends to dissolve the $CsPbX_3$ QDs, causing the strategy to remain relatively underdeveloped. Here, we present an improved hot-injection method that can facilitate the epitaxial growth of $CsPb_2Br_5$ shell on the surface of $CsPbBr_3$ QDs, and, by doping Sr^{2+} ions to passivate the defects of the QDs, $CsPbBr_3$@$CsPb_2Br_5$:Sr core-shell microplates have been obtained. The composites have enhanced optical properties and stability. Density Functional Theory (DFT) calculations show that this is benefited from the introduction of Sr which widens the bandgap of $CsPbBr_3$ and $CsPb_2Br_5$, leading to the formation of a quantum well structure between the two, significantly improving the quantum yields of the samples. Finally, the white light emitting diodes prepared using the composite have high luminous efficiency and long-term operational stability.

1. Introduction

Cesium lead halide ($CsPbX_3$ (X = Cl, Br, I)) perovskite quantum dots (QDs) have attracted great interest from researchers due to their outstanding optical properties [1–4]. The material has a high photoluminescence quantum yield (PLQY) and tunable optical properties, making it suitable for various optoelectronic applications such as lasers [5], high-efficiency light-emitting diodes (LEDs) [6] and solar cells [7]. However, defects such as high defect state densities, easily desorbed surface ligands, and worrisome stability have hindered the commercialization of $CsPbX_3$ QDs [8–10]. The core-shell structure provides options for improving the stability of $CsPbX_3$ QDs [11,12]. However, this strategy will easily deteriorate the optical properties of the QDs, because the presence of heterogeneous shells tends to lead to self-absorption/reabsorption effects [13], and, the complex post-processing often decomposes the fragile $CsPbX_3$ QDs [14,15].

The introduction of impurity ions to improve the optical properties of $CsPbX_3$ QDs has been proved to be an effective means [16,17]. For example, Pan et al. obtained perovskite nanocrystals with unit quantum yield by doping various lanthanide ions into the lattice of $CsPbCl_3$ [18]. In addition, it has been shown that impurity ions such as Sn [19,20], Cd [21,22], and Zn [23,24] can all significantly improve the luminous efficiency of $CsPbX_3$ QDs. Except for the improvement of quantum yield, impurity ions also enable the versatility of $CsPbX_3$ QDs. For example, Mn^{2+} dopants that have been widely reported, in which the $PbCl_2$ and $MnCl_2$ precursors are mixed in desired ratio, can obtain perovskite nanocrystals with Mn^{2+} emission [25–27]. However, all such doping strategies face an unavoidable problem: due to ionic radius and surface charge differences, impurity ions have the potential to cause the host to lose its inherent crystal structure and emission [28]. Therefore, a convenient improvement strategy is needed to enhance the radiative recombination efficiency of $CsPbX_3$ QDs while maintaining the stability of the perovskite crystal structure.

In this work, we present an improved thermal injection method to epitaxially grow $CsPb_2Br_5$ shell on the surface of $CsPbBr_3$ QDs, which significantly enhances the stability of the QDs. Further, through the

* Corresponding author.
E-mail address: mqwang@xjtu.edu.cn (M. Wang).

https://doi.org/10.1016/j.jlumin.2024.120785
Received 22 May 2024; Received in revised form 26 June 2024; Accepted 10 July 2024
Available online 10 July 2024
0022-2313/© 2024 Elsevier B.V. All rights are reserved, including those for text and data mining, AI training, and similar technologies.

introduction of Sr^{2+} impurity ions, $CsPbBr_3$@$CsPb_2Br_5$:Sr core-shell microplates with high PLQY (96 %) are obtained. This strategy balances stability and luminous efficiency and avoids complex post-processing. Our study demonstrates that Sr^{2+} widens the band gap of $CsPbBr_3$ and $CsPb_2Br_5$ promoting the formation of type-I heterojunctions between them. This allows more carriers to recombine in the energy band of the $CsPbBr_3$ QDs, which significantly improves the radiative recombination efficiency of the samples. Benefiting from the advantages of high luminous efficiency and high stability of the composites, the prepared white light-emitting diodes (WLED) maintain more than 90 % of the PL intensity after 15 h of continuous operation in high temperature environment (105 °C). Our work provides many new possibilities for the application of $CsPbX_3$ perovskite quantum dots.

2. Results and discussion

2.1. Morphology and crystal structure of the CCS composites

In this paper, Sr-doped $CsPbBr_3$@$CsPb_2Br_5$ core-shell microplates are obtained in one step by using the conventional hot-injection method through extending the reaction time and controlling the ratio of precursors. Specifically, a total of 0.3 mmol of $SrBr_2$ and $PbBr_2$ was dissolved in 1-octadecene. Subsequently, low concentrations of Cs+ (≈0.1 mmol) were injected at 170 °C for 1 h of reaction. The epitaxial growth of $CsPb_2Br_5$ on the surface of $CsPbBr_3$ was induced by Pb-rich environment to obtain $CsPbBr_3$@$CsPb_2Br_5$:Sr core-shell microplates (denoted as CCS composites). The detailed procedure could be found in the experimental section of the supporting information.

First, we observed the morphology of the samples at different reaction times to reveal the growth process of $CsPb_2Br_5$ on the $CsPbBr_3$ surface. In the first 5 S of the reaction, scanning electron microscopy (SEM) and transmission electron microscopy (TEM) observed the sample was uniform cubic $CsPbBr_3$:Sr QDs (Figs. S1a and b), tentatively suggesting that the introduction of Sr^{2+} would not alter the inherent crystal structure of $CsPbBr_3$ QDs. Further, when the reaction time was extended to 30 min, these $CsPbBr_3$:Sr QDs were no longer uniformly spread out on the silicon substrate, but gradually agglomerated into circular sheets with a size of about 5 μm (Fig. 1a1). High-resolution SEM images showed that circular sheets consisted of the 2D thin film-like substrate and a large number of QDs embedded inside it (Fig. 1a2). The substrate was identified as $CsPb_2Br_5$ by X-ray diffraction (XRD) (Fig. S2). Subsequently, TEM displayed this embedded structure clearly, and it could be found that the external $CsPb_2Br_5$ had completely encapsulated the internal QDs, insulating them from the surrounding environment (Fig. 1a3). Finally, when the reaction time was extended to 1 h, these circular sheets no longer adhered to each other, but evolved into monodisperse octagonal microplates (Fig. 1b1) with an average size of 5.36 μm (Fig. S3a). Moreover, in contrast to the samples reacted for only 30 min, these octagonal microplates had smooth surfaces, tentatively inferring that all QDs were completely encapsulated inside $CsPb_2Br_5$ (Fig. 1b2). The corresponding TEM images showed that the $CsPb_2Br_5$ formed a dense shell, with thicknesses ranging from 14 to 36 nm (Fig. 1b3), and numerous tiny $CsPbBr_3$:Sr QDs existed in the interior of microplates, with an average size of 14.66 nm (Fig. S3b). Finally, elemental mapping of the sample showed that Cs:Pb:Sr:Br was 1:1.3:1:3.6, with no aggregation due to prolonged high temperatures or Pb-rich environments (Fig. 1c and Table S1). It was worth noting that since Sr was uniformly distributed in the whole grain, the $CsPb_2Br_5$ shell was also partially doped with Sr^{2+} ions, which was also proved by the subsequent XRD results.

Subsequently, we analyzed the crystal structures of the CCS composites by high-resolution TEM (HRTEM). First, the composites could

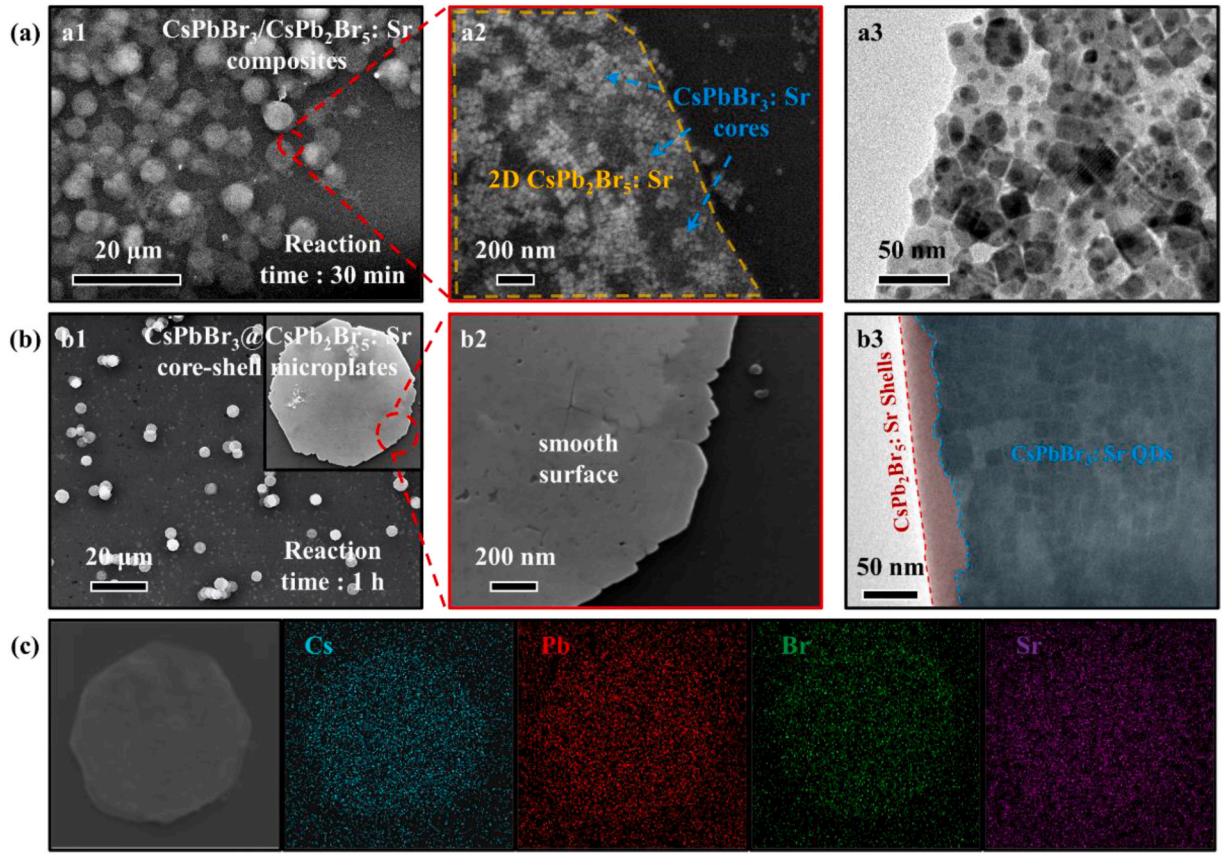

Fig. 1. (a) SEM and TEM images of the samples after 30 min reaction. (b) SEM and TEM images of the sample after 1 h reaction. (c) Elemental mapping of CCS composites.

easily distinguish two different lattice fringes. Among them, 0.76 nm corresponds to the (002) plane of the tetragonal (β) $CsPb_2Br_5$; 0.59 nm corresponds to the (100) plane of the cubic (α) $CsPbBr_3$ (Fig. 2a). The corresponding selected-area electron diffraction (SAED) image consisted of clear single-crystal diffraction spots and polycrystalline rings (Fig. 2b), suggesting that the structure of the CCS composites was a $CsPb_2Br_5$:Sr single-crystal shell encapsulating a large number of $CsPbBr_3$:Sr QDs, and they both had excellent crystallinity. Further, X-ray photoelectron spectroscopy (XPS) was used to determine the chemical composition of the CCS composites (Fig. 2c). Firstly, compared with $CsPbBr_3$, both $CsPbBr_3$:Sr and CCS composites showed significant Sr signals, demonstrating that Sr^{2+} successfully replaced Pb^{2+} in the lattice (Fig. 2d). In addition, the Cs 3d, Pb 4f, and Br 3d signals of $CsPbBr_3$:Sr were almost unchanged, indicating that the effect of doped Sr^{2+} on the binding energy of the samples could be negligible (Fig. 2e–g). However, the signals of Pb 4f, Cs 3d, and Br 3d of the CCS composites were slightly shifted toward higher binding energy (ΔeV≈0.2–0.3 eV), suggesting that after passivation of the $CsPb_2Br_5$ shell, the electron density of the $CsPbBr_3$ cores was decreased. This phenomenon was consistent with previous reports, attributing it to the strong sharing of Pb atoms between 0D $CsPbBr_3$ and 2D $CsPb_2Br_5$ [29,30]. Similarly, we compared the XRD patterns of $CsPbBr_3$ QDs, $CsPbBr_3$:Sr QDs and CCS composites. The results showed that the $CsPbBr_3$ and $CsPbBr_3$:Sr QDs were cubic $CsPbBr_3$ (PDF#54–0752) with no other phases due to Sr doping (Fig. 2h). But the CCS composites exhibited a diffraction peak of the tetragonal $CsPb_2Br_5$ (002) plane at 11.66° (PDF#25–0211), and the peak had a sharp shape which was consistent with the micrometer grain size of the samples.

Finally, we compared the PL spectra and time-resolved PL decays of the three to demonstrate that the CCS composites had the best optical properties. First, PL spectra showed that after doping with Sr^{2+}, the PL peak position of $CsPbBr_3$ QDs was blue-shifted from 519 nm to 502 nm, whereas the PL peak position of the CCS composites was red-shifted to 505 nm, exhibiting enhanced optical properties (Fig. 2i). Among them, the blue shift of the PL position due to Sr^{2+} might be related to the energy band change, which was subsequently discussed in the calculation part; while the red shift of the CCS composites was caused by the increase of the QDs size due to the prolonged high-temperature reaction. Further, the time-resolved PL decays showed that the PL lifetime of $CsPbBr_3$:Sr QDs was enhanced from 17.79 ns to 20.50 ns; whereas the PL lifetime of the CCS composites was 46.38 ns, which was ~2.6 times for $CsPbBr_3$ QDs and ~2.3 times for $CsPbBr_3$:Sr QDs (Fig. 2j). This phenomenon demonstrated that both Sr^{2+} and $CsPb_2Br_5$ shells were effective in prolonging the PL lifetimes of $CsPbBr_3$ QDs, improving the radiative recombination efficiency [31].

2.2. *Optical properties and stability of the CCS composites with different Sr^{2+} doping concentrations*

Further, we investigated the optical properties of the CCS composites with different Sr doping concentrations in order to find the optimal

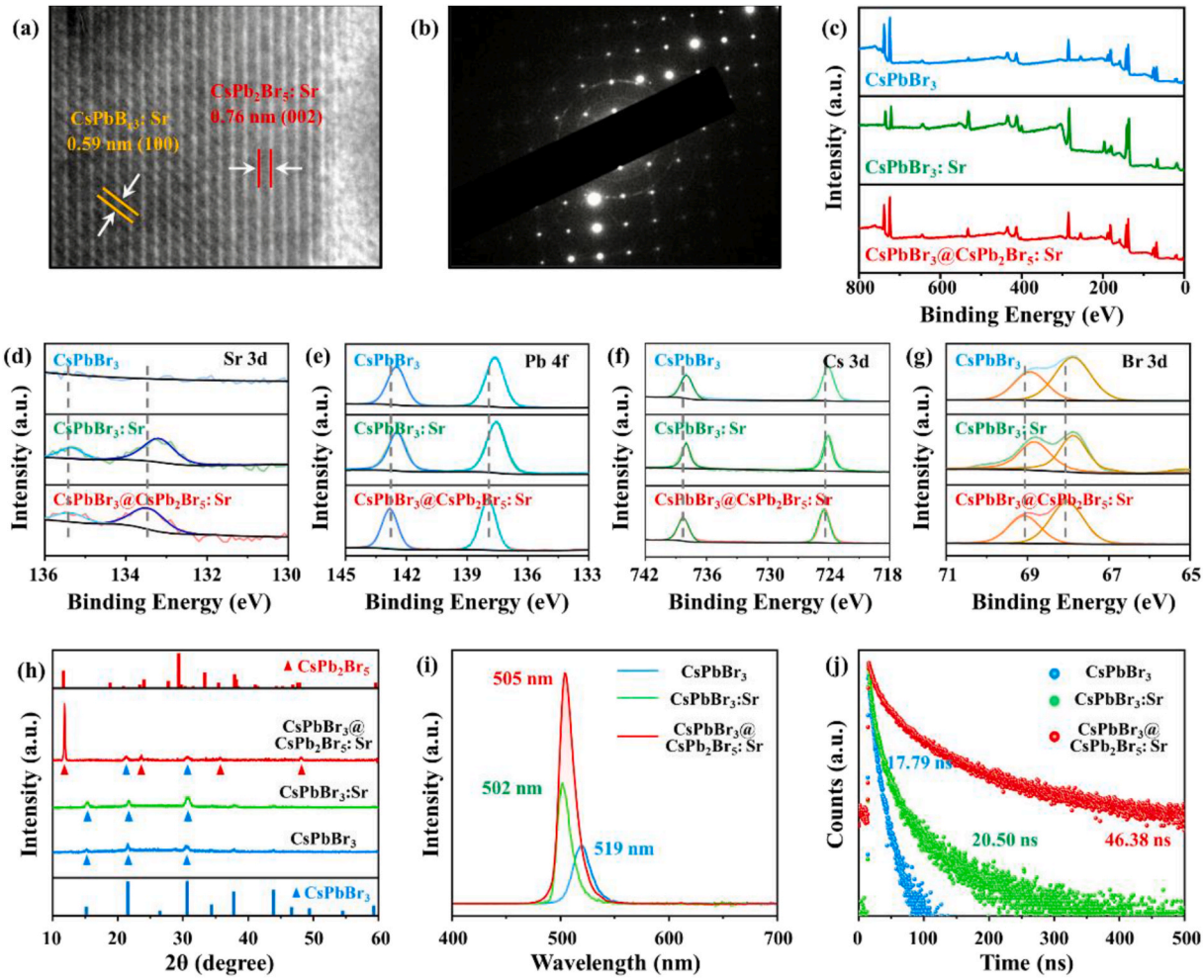

Fig. 2. (a) HRTEM image and (b) SAED pattern of CCS composites. (c) Comparison of XPS spectra of $CsPbBr_3$, $CsPbBr_3$:Sr and CCS composites. High-resolution XPS spectra of (d) Sr 3d, (e) Pb 4f, (f) Cs 3d, and (g) Br 3d. Comparison of (h) XRD patterns, (i) PL spectra (λ = 365 nm) and (j) time-resolved PL decays of CCS composites, $CsPbBr_3$:Sr QDs and $CsPbBr_3$ QDs.

doping ratio. First, the PL spectra showed that the peak position of the $CsPbBr_3$ cores was blue-shifted (518 nm→500 nm) with increasing Sr^{2+} concentration, and the PL intensity peaked at Sr/Pb = 0.8, then followed by a decreasing trend (Fig. 3a and Table S2). The corresponding PLQY has similar results, where the CCS composites with Sr/Pb = 0.8 exhibited a high quantum yield of 96 % (Fig. 3b). Compared to the $CsPbBr_3$ QDs (Sr/Pb = 0), PLQY was enhanced by 43 % (PLQY = 53 %); compared to $CsPbBr_3$:Sr (Sr/Pb = 0.6), PLQY was enhanced by 29 % (PLQY = 67 %). Subsequently, the corresponding XRD results showed that two kinds of diffraction peaks were clearly distinguished for all sample, corresponding to the cubic $CsPbBr_3$ and the tetragonal $CsPb_2Br_5$ (Fig. 3c). This phenomenon proved that these "foreign" atoms would not affect the inherent crystal structure of $CsPbBr_3$ or $CsPb_2Br_5$ even at high Sr doping concentration (Sr/Pb = 1.0). Moreover, all the diffraction peaks of $CsPbBr_3$ and $CsPb_2Br_5$ were slightly shifted to the large angle direction with the increase of Sr^{2+}, and this lattice shrinkage proved that Sr^{2+} was existed not only in the internal $CsPbBr_3$ but also in the $CsPb_2Br_5$ shell. Further, the time-dependent PL decays showed the effect of doping concentration on the carrier recombination process. The PL decay curves for all samples could be fitted well by bi-exponential decay model. Among them, the fast decay was related to trap-assisted recombination, while the slow decay was related to the radiative recombination. Analysis of the fitted data revealed that the radiative recombination efficiency A_2 was enhanced with increasing Sr^{2+} concentration, peaking at Sr/Pb = 0.8 (Fig. 3d and Table S3). At this point, the CCS composites possessed the longest PL lifetime (46.38 ns). This result was almost consistent with the trend of PLQY, further confirming that the introduction of Sr^{2+} was beneficial to improve the PLQY of the samples. With the further increasing of Sr^{2+} concentration (Sr/Pb = 1.0), the non-radiative recombination efficiency A1 was significantly increased, attributed to the excess doping leading to the additional interstitial atoms, which elevated the density of trap states.

Finally, we evaluated the stability of the CCS composites (Sr/Pb = 0.8) to demonstrate that the materials had the basis for practical applications [32]. First, the thermal stability results showed that after six heating-cooling cycles (25–140 °C), the CCS composites could retain 93.3 % of the initial PL intensity; $CsPbBr_3$@$CsPb_2Br_5$ could retain 91.8 % of the initial PL intensity; whereas the $CsPbBr_3$ QDs remained only 34.9 % (Fig. S4a). The photostability had similar results (Fig. S4b). After passivation of the $CsPb_2Br_5$ shell, the irradiation resistance of the samples was significantly improved. Further, the CCS composites possessed a larger water contact angle than the $CsPbBr_3$ and $CsPbBr_3$@$CsPb_2Br_5$ films, making the samples more hydrophobic and the water could not easily penetrate into the materials (Fig. 3e). Therefore, the CCS composites and $CsPbBr_3$@$CsPb_2Br_5$ retained more than 95 % of the initial PL intensity after 12 days of immersion, whereas the $CsPbBr_3$:Sr QDs were almost quenched after a few hours of immersion (Fig. 3f). It was attributed to the high enthalpy of decomposition of $CsPb_2Br_5$ in water, which resulted in the surprising water stability of the CCS composites [33,34].

2.3. Energy band structure of the CCS composites

Since Sr^{2+} was uniformly distributed in the $CsPbBr_3$ and $CsPb_2Br_5$ shell, we calculated the electronic structures of the two materials doped with Sr^{2+}, and explained the effect of photo-enhancement of the Sr^{2+} ions and the $CsPb_2Br_5$ shell through the perspective of energy bands. Fig. 4a–d showed the calculated models for the two materials, respectively, with a doping concentration of Sr/Pb = 0.8, and, considering the symmetry of the crystal structure, the Sr^{2+} ions were set as far away from each other as possible. Subsequently, Fig. 4b exhibited the electronic structure of $CsPbBr_3$:Sr. The material had a band gap of 2.74 eV, which was significantly increased compared to undoped $CsPbBr_3$ (1.80 eV, Fig. S5a). Meanwhile, the projected density of states indicated that the valence band maximum (VBM) of $CsPbBr_3$:Sr was mainly composed of Br p orbitals, with a slight contribution from Pb s orbitals; while the conduction band minimum (CBM) was mainly composed of Pb p orbitals, with a negligible contribution from Sr orbitals (Fig. 4c). Previous reports suggested that the band gap of ABX_3 perovskite might be widened by the decrease in electronegativity of the B-site cations

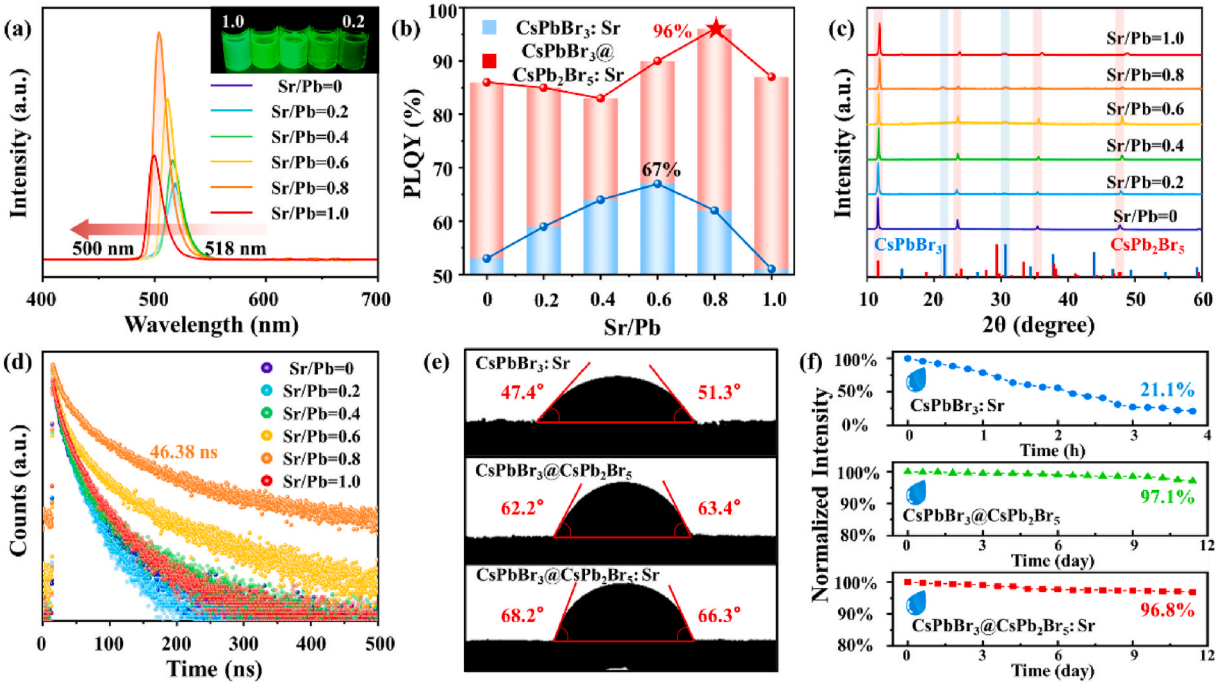

Fig. 3. Comparison of (a) PL spectra (λ = 365 nm), (b) PLQY, (c) XRD patterns, and (d) time-resolved PL decays of CCS composites with different Sr^{2+} doping concentrations. Where, Sr/Pb = 0 represented the non-Sr^{2+} doped $CsPbBr_3$@$CsPb_2Br_5$ composites. Comparison of (e) water contact angle and (f) water stability of $CsPbBr_3$:Sr QDs (Sr/Pb = 0.8), $CsPbBr_3$@$CsPb_2Br_5$ composites and CCS composites (Sr/Pb = 0.8). *Normalized Intensity* = $I/I_0 \times 100$ %, where, I was PL intensity of samples after immersion and I_0 was the initial PL intensity before immersion.

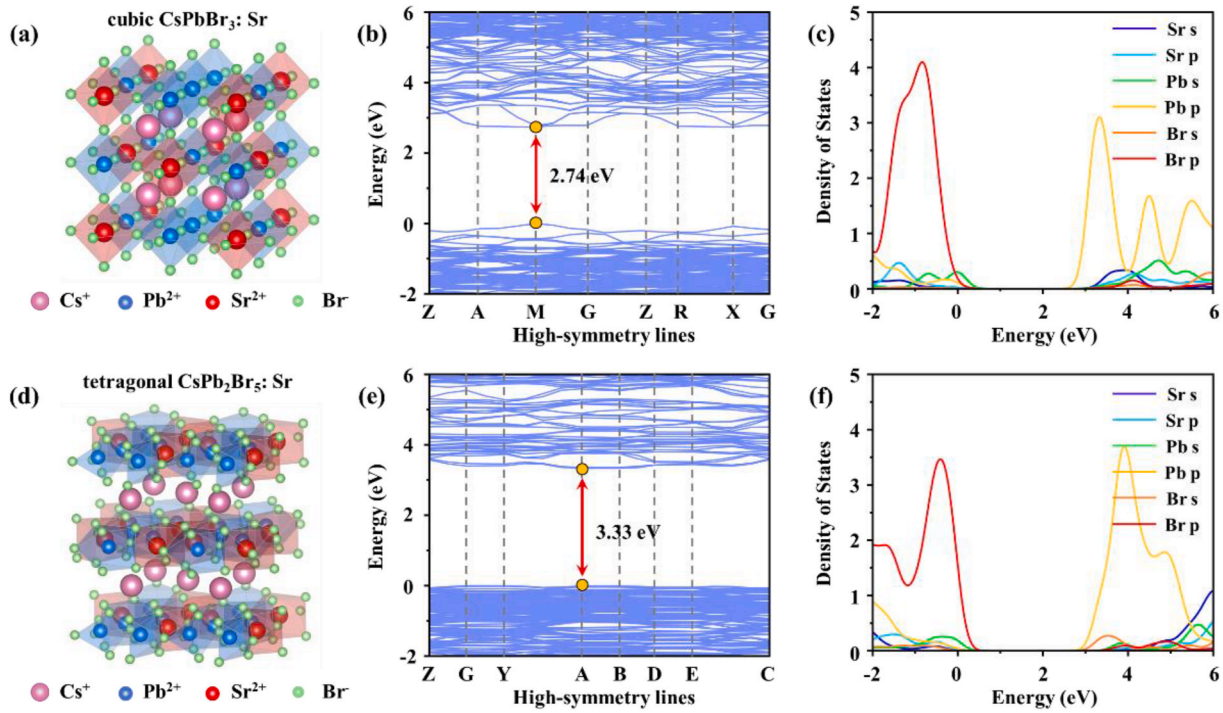

Fig. 4. (a) Atomic model, (b) electronic structure and (c) projected density of states of Sr-doped (Sr/Pb = 0.8) $CsPbBr_3$ core. (d) Atomic model, (e) electronic structure and (c) projected density of states of Sr-doped (Sr/Pb = 0.8) $CsPb_2Br_5$ shell.

[35–37], where the electronegativity of Sr^{2+} (0.99) was weaker than the electronegativity of Pb^{2+} (1.55), which might be one of the reasons. Further, the substitution of Sr^{2+} (ionic radius: 118 p.m.) for Pb^{2+} (ionic radius: 119 p.m.) would result in reduction of the unit cell volume, and the Pb–Br bond became shorter, which enhanced the interaction between the Pb and Br orbitals. Since the CBM of $CsPbBr_3$ was composed of the antibonding combinations between Pb (6p) and Br (4p) orbitals, it would shift to higher energies with stronger interactions, resulting in a wider band gap [38]. In summary, the electronegativity increase and lattice contraction collectively lead to the band gap broadening of Sr^{2+} doped $CsPbBr_3$ without the introduction of defective energy levels. Calculations for the $CsPb_2Br_5$ shell were in agreement with them, with an increase of 0.29 eV in the band gap after Sr^{2+} doping (undoped: 3.04 eV, Fig. S5b; doped: 3.33 eV, Fig. 4e). Moreover, the Sr orbitals barely contribute to both CBM and VBM, and the increase in band gap was equally attributed to the increased electronegativity and lattice contraction (Fig. 4f). Therefore, we could obtain the whole energy band structure of the composites. The results showed that the CBM of $CsPb_2Br_5$ was higher than the CBM of $CsPbBr_3$; the VBM of $CsPb_2Br_5$ was lower than the VBM of $CsPbBr_3$. A typical type-I heterojunction was formed between the two, which effectively confined the electrons and holes in the energy band of $CsPbBr_3$, improving the quantum yield (Fig. S6).

2.4. Optical properties and stability of WLED

Currently, the WLED is one of the most important applications of $CsPbX_3$ perovskite QDs, and the optical properties of the device determines the prospect of material [39,40]. We used the CCS composites with Sr/Pb = 0.8 as green light source and the $CsPb(Br/I)_3$@$CsPb_2(Br/I)_5$:Sr composites with 624 nm emission by anion exchange method as red light source. Subsequently, two phosphors were made into polymer films and integrated onto a 450 nm blue chip to fabricate WLED (denoted as Sr-LED). Futher, we also prepared WLED using $CsPbX_3$ QDs for comparison (denoted as QDs-LED).

First, the PL spectra of the Sr-LED showed that the device could clearly distinguish the emission of blue (450 nm), green (505 nm), and red (624 nm) phosphors (Fig. 5a), corresponding to the 450 nm blue chip, the CCS composites, and the $CsPb(Br/I)_3$@$CsPb_2(Br/I)_5$:Sr composites, respectively. The chromaticity coordinate of the Sr-LED were (0.318, 0.326), exhibiting pure white light emission (Fig. 5b). Further, the highest luminous efficiency of the Sr-LED was 132.61 lm/W (26 mA); the highest color rendering index (CRI) reached 97 (20 mA) (Fig. 5c and d). In contrast, the highest luminous efficiency of the QDs-LED was only 85.17 lm/W, and the CRI gradually decreased with the rise of the drive current, eventually leaving only 39. Finally, since optoelectronic devices inevitably generated high temperatures during continuous operation, this could lead to thermal decomposition of $CsPbX_3$ QDs [41,42]. Therefore, we recorded the surface temperature and PL spectra of Sr-LED at different operating times to demonstrate that the CCS composites had long-term operational stability. The results showed that the surface temperature of the Sr-LED increased to more than 100 °C after only 1 h of work, and remained at 100–106 °C for the following 3–15 h (Fig. 5e). Obviously, such high temperature environments would dramatically deteriorate the optical properties of QDs. However, the PL intensity of Sr-LED retained more than 90 % of the initial PL intensity after 15 h of continuous operation (where, the PL intensity of red light decayed by ~9.1 %; the PL intensity of green light decayed by ~5.4 %), and the peak position had no significant shift (Fig. 5f). To conclude, $CsPbBr_3$ QDs passivated by Sr^{2+} and $CsPb_2Br_5$ shell could provide a new option for the application of perovskite materials in the field of optoelectronics.

3. Conclusions

We presented an improved hot-injection method to obtain $CsPbBr_3$@$CsPb_2Br_5$:Sr microplates with the core-shell structure by controlling the precursor ratio and the reaction time. After the co-passivation of Sr^{2+} and $CsPb_2Br_5$ shell, the composites exhibited 96 % PLQY and excellent stability, which was in sharp contrast to the unimproved $CsPbBr_3$ QDs. Subsequently, DFT calculations showed that the Sr-doped $CsPbBr_3$ and $CsPb_2Br_5$ bandgaps were obviously increased and

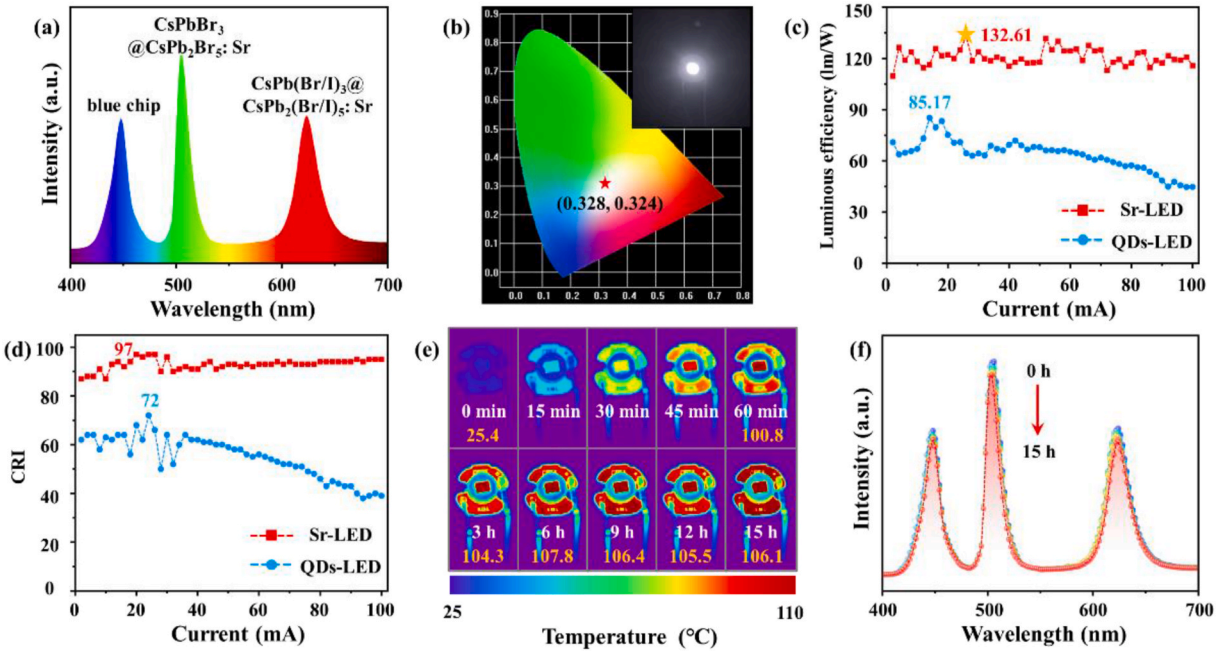

Fig. 5. (a) PL spectra and (b) chromaticity coordinate of Sr-LED at 20 mA drive current. The inset showed the photo of the device. Comparison of (c) Luminous efficiency and (d) CRI of Sr-LED and QDs-LED at 2–100 mA driving current. (e) Surface temperature and (f) PL spectra of Sr-LED continuously operated for 15 h at 20 mA driving current.

the PL peaks were blueshifted, which were attributed to the increased electronegativity and lattice contraction induced by the substitution of Sr^{2+} for Pb^{2+}. Further, typical type-I heterojunctions were formed between $CsPbBr_3$ and $CsPb_2Br_5$, which significantly improved the radiative recombination efficiency of the QDs. Finally, the WLED fabricated using the composites possessed the luminous efficiency of 132.61 lm/W and the color rendering index of 97, and the PL intensity remained above 90 % after 15 h of continuous operation in 105 °C high-temperature environment. This high luminous efficiency and high stability of $CsPbBr_3$@$CsPb_2Br_5$:Sr core-shell microplates are beneficial for realizing various applications in optoelectronics.

CRediT authorship contribution statement

Chen Zhang: Writing – original draft, Software, Methodology, Investigation, Data curation. **Minqiang Wang:** Supervision, Project administration, Funding acquisition. **Zheyuan Da:** Software, Methodology, Data curation. **Jindou Shi:** Writing – review & editing, Supervision, Investigation. **Junnan Wang:** Writing – review & editing, Methodology, Investigation. **Qing Yao:** Writing – review & editing, Software. **Nikolai V. Gaponenko:** Supervision, Resources, Project administration.

Declaration of competing interest

The authors declare that they have no known competing financial interests or personal relationships that could have appeared to influence the work reported in this paper.

Data availability

Data will be made available on request.

Acknowledgment

This work was supported by the National Key R&D Program of China (2022YFE0122500 and 2019YFB1503200), National Natural Science Foundation of China (NSFC, 52161145103 and 61774124), 111 Program (No. B14040), and Shaanxi Provincial Key Research and Development Program (No. 2021GXLH-Z-084). The authors thank Ms. Dan He at Instrument Anaysis Center of Xi'an Jiaotong University for her help with the time-resolved PL analysis.

Appendix A. Supplementary data

Supplementary data to this article can be found online at https://doi.org/10.1016/j.jlumin.2024.120785.

References

[1] L. Protesescu, S. Yakunin, M.I. Bodnarchuk, F. Krieg, R. Caputo, C.H. Hendon, R. X. Yang, A. Walsh, M.V. Kovalenko, Nanocrystals of cesium lead halide perovskites ($CsPbX_3$, X = Cl, Br, and I): novel optoelectronic materials showing bright emission with wide color gamut, Nano Lett. 15 (6) (2015) 3692–3696, https://doi.org/10.1021/nl5048779.

[2] Q. Lin, S. Bernardi, B. Shabbir, Q. Ou, M. Wang, W. Yin, S. Liu, A.S.R. Chesman, S. O. Fürer, G. Si, N. Medhekar, J. Jasieniak, A. Widmer-Cooper, W. Mao, U. Bach, Phase-control of single-crystalline inorganic halide perovskites via molecular coordination engineering, Adv. Funct. Mater. 32 (16) (2021), https://doi.org/10.1002/adfm.202109442.

[3] M. Liu, J. Zhao, Z. Luo, Z. Sun, N. Pan, H. Ding, X. Wang, Unveiling solvent-related effect on phase transformations in CsBr–$PbBr_2$ system: coordination and ratio of precursors, Chem. Mater. 30 (17) (2018) 5846–5852, https://doi.org/10.1021/acs.chemmater.8b00537.

[4] V.K. Ravi, G.B. Markad, A. Nag, Band edge energies and excitonic transition probabilities of colloidal $CsPbX_3$ (X = Cl, Br, I) perovskite nanocrystals, ACS Energy Lett. 1 (4) (2016) 665–671, https://doi.org/10.1021/acsenergylett.6b00337.

[5] Y. Bai, M. Hao, S. Ding, P. Chen, L. Wang, Surface chemistry engineering of perovskite quantum dots: strategies, applications, and perspectives, Adv Mater 34 (4) (2022) e2105958, https://doi.org/10.1002/adma.202105958.

[6] K. Lin, J. Xing, L.N. Quan, F.P.G. de Arquer, X. Gong, J. Lu, L. Xie, W. Zhao, D. Zhang, C. Yan, W. Li, X. Liu, Y. Lu, J. Kirman, E.H. Sargent, Q. Xiong, Z. Wei, Perovskite light-emitting diodes with external quantum efficiency exceeding 20 percent, Nature 562 (7726) (2018) 245–248, https://doi.org/10.1038/s41586-018-0575-3.

[7] E. Jang, H. Jang, Review: quantum dot light-emitting diodes, Chem Rev 123 (8) (2023) 4663–4692, https://doi.org/10.1021/acs.chemrev.2c00695.

[8] K. Vighnesh, S. Wang, H. Liu, A.L. Rogach, Hot-injection synthesis protocol for green-emitting cesium lead bromide perovskite nanocrystals, ACS Nano 16 (12) (2022) 19618–19625, https://doi.org/10.1021/acsnano.2c11689.

[9] J. Pan, Y. Shang, J. Yin, M. De Bastiani, W. Peng, I. Dursun, L. Sinatra, A.M. El-Zohry, M.N. Hedhili, A.H. Emwas, O.F. Mohammed, Z. Ning, O.M. Bakr, Bidentate ligand-passivated $CsPbI_3$ perovskite nanocrystals for stable near-unity photoluminescence quantum yield and efficient red light-emitting diodes, J. Am. Chem. Soc. 140 (2) (2018) 562–565, https://doi.org/10.1021/jacs.7b10647.

[10] Z. Zhang, Y. Zhu, W. Wang, W. Zheng, R. Lin, F. Huang, Growth, characterization and optoelectronic applications of pure-phase large-area $CsPb_2Br_5$ flake single crystals, J. Mater. Chem. C 6 (3) (2018) 446–451, https://doi.org/10.1039/c7tc04834c.

[11] M. He, Q. Zhang, F. Carulli, A. Erroi, W. Wei, L. Kong, C. Yuan, Q. Wan, M. Liu, X. Liao, W. Zhan, L. Han, X. Guo, S. Brovelli, L. Li, Ultra-stable, solution-processable $CsPbBr_3$-SiO_2 nanospheres for highly efficient color conversion in micro light-emitting diodes, ACS Energy Lett. 8 (1) (2022) 151–158, https://doi.org/10.1021/acsenergylett.2c02062.

[12] Q. Zhong, M. Cao, H. Hu, D. Yang, M. Chen, P. Li, L. Wu, Q. Zhang, One-pot synthesis of highly stable $CsPbBr_3$@SiO_2 core-shell nanoparticles, ACS Nano 12 (8) (2018) 8579–8587, https://doi.org/10.1021/acsnano.8b04209.

[13] M. Fan, J. Huang, L. Turyanska, Z. Bian, L. Wang, C. Xu, N. Liu, H. Li, X. Zhang, C. Zhang, X. Yang, Efficient all-perovskite white light-emitting diodes made of in situ grown perovskite-mesoporous silica nanocomposites, Adv. Funct. Mater. (2023) 2215032, https://doi.org/10.1002/adfm.202215032.

[14] Z.J. Li, E. Hofman, J. Li, A.H. Davis, C.H. Tung, L.Z. Wu, W. Zheng, Photoelectrochemically active and environmentally stable $CsPbBr_3$/TiO_2 core/shell nanocrystals, Adv. Funct. Mater. 28 (1) (2017), https://doi.org/10.1002/adfm.201704288.

[15] Y. Tong, Q. Wang, E. Mei, X. Liang, W. Gao, W. Xiang, One-pot synthesis of $CsPbX_3$ (X = Cl, Br, I)@Zeolite: a potential material for wide-color-gamut backlit displays and upconversion emission, Adv. Opt. Mater. 9 (11) (2021), https://doi.org/10.1002/adom.202100012.

[16] L. Ruan, Y. Zhang, NIR-excitable heterostructured upconversion perovskite nanodots with improved stability, Nat. Commun. 12 (1) (2021) 219, https://doi.org/10.1038/s41467-020-20551-z.

[17] C. Chen, T. Xuan, W. Bai, T. Zhou, F. Huang, A. Xie, L. Wang, R.-J. Xie, Highly stable $CsPbI_3$:Sr^{2+} nanocrystals with near-unity quantum yield enabling perovskite light-emitting diodes with an external quantum efficiency of 17.1, Nano Energy 85 (2021), https://doi.org/10.1016/j.nanoen.2021.106033.

[18] G. Pan, X. Bai, D. Yang, X. Chen, P. Jing, S. Qu, L. Zhang, D. Zhou, J. Zhu, W. Xu, B. Dong, H. Song, Doping lanthanide into perovskite nanocrystals: highly improved and expanded optical properties, Nano Lett. 17 (12) (2017) 8005–8011, https://doi.org/10.1021/acs.nanolett.7b04575.

[19] C. Duan, F. Zou, Q. Wen, M. Qin, J. Li, C. Chen, X. Lu, L. Ding, K. Yan, A bifunctional carbazide additive for durable $CsSnI_3$ perovskite solar cells, Adv Mater 35 (26) (2023) e2300503, https://doi.org/10.1002/adma.202300503.

[20] C. Kang, H. Rao, Y. Fang, J. Zeng, Z. Pan, X. Zhong, Antioxidative stannous oxalate derived lead-free stable $CsSnX_3$ (X=Cl, Br, and I) perovskite nanocrystals, Angew Chem. Int. Ed. Engl. 60 (2) (2021) 660–665, https://doi.org/10.1002/anie.202011569.

[21] A. Swarnkar, V.K. Ravi, A. Nag, Beyond colloidal cesium lead halide perovskite nanocrystals: analogous metal halides and doping, ACS Energy Lett. 2 (5) (2017) 1089–1098, https://doi.org/10.1021/acsenergylett.7b00191.

[22] Z. Wu, B. Du, G. Tong, H. Zhang, Y. Zhang, J. Xia, Z. Zhao, Highly luminescent and stable inorganic perovskite micro-nanocomposites for crucial information encryption and decryption, Chem. Eng. J. 428 (2022), https://doi.org/10.1016/j.cej.2021.131016.

[23] D. Li, P. Xie, Y. Zhang, Y. Meng, Y. Chen, Y. Zheng, W. Wang, D. Yin, B. Li, Z. Wu, C. Lan, S. Yip, D. Lei, F.R. Chen, J.C. Ho, Phase engineering for stability of $CsPbI_3$ nanowire optoelectronics, Adv. Funct. Mater. (2024), https://doi.org/10.1002/adfm.202314309.

[24] S. Zhang, L. Yuan, H. Liu, G. Zhou, W. Ding, Z. Qin, X. Li, S. Wang, Tunable white light-emitting devices based on unilaminar high-efficiency Zn^{2+}-doped blue $CsPbBr_3$ quantum dots, J. Phys. Chem. Lett. 12 (35) (2021) 8507–8512, https://doi.org/10.1021/acs.jpclett.1c02519.

[25] W.J. Mir, M. Jagadeeswararao, S. Das, A. Nag, Colloidal Mn-doped cesium lead halide perovskite nanoplatelets, ACS Energy Lett. 2 (3) (2017) 537–543, https://doi.org/10.1021/acsenergylett.6b00741.

[26] J. Shi, M. Wang, C. Zhang, J. Wang, Y. Zhou, Y. Xu, N.V. Gaponenko, Enhanced stability of lead-free double perovskite $Cs_2Na_{1-x}Bi_{1-x}Mn_{2x}Cl_6$ microcrystals and their optoelectronic devices under high humidity environment by SiO_2 encapsulation, Mater. Today Chem. 29 (2023), https://doi.org/10.1016/j.mtchem.2023.101480.

[27] A.K. Guria, S.K. Dutta, S.D. Adhikari, N. Pradhan, Doping Mn^{2+} in lead halide perovskite nanocrystals: successes and challenges, ACS Energy Lett. 2 (5) (2017) 1014–1021, https://doi.org/10.1021/acsenergylett.7b00177.

[28] L. Wu, Y. Wang, M. Kurashvili, A. Dey, M. Cao, M. Doblinger, Q. Zhang, J. Feldmann, H. Huang, T. Debnath, Interfacial manganese-doping in $CsPbBr_3$ nanoplatelets by employing a molecular shuttle, Angew Chem. Int. Ed. Engl. 61 (15) (2022) e202115852, https://doi.org/10.1002/anie.202115852.

[29] L. Ding, B. Borjigin, Y. Li, X. Yang, X. Wang, H. Li, Assembling an affinal 0D $CsPbBr_3$/2D $CsPb_2Br_5$ architecture by synchronously in situ growing $CsPbBr_3$ QDs and $CsPb_2Br_5$ nanosheets: enhanced activity and reusability for photocatalytic CO_2 reduction, ACS Appl. Mater. Interfaces 13 (43) (2021) 51161–51173, https://doi.org/10.1021/acsami.1c17870.

[30] I. Rosa-Pardo, A. Ciccone, R. Arenal, R.E. Galian, J. Pérez-Prieto, One-pot synthesis of stable $CsPbBr_3$@$CsPb_2Br_5$ core–shell heteronanocrystals with controlled permeability to halide ions, Chem. Mater. 35 (17) (2023) 7011–7019, https://doi.org/10.1021/acs.chemmater.3c01280.

[31] J. Deng, J. Xun, W. Shen, M. Li, R. He, Phase regulation of $CsPb_2Br_5$/$CsPbBr_3$ perovskite nanocrystals by doping with divalent cations: implications for optoelectronic devices with enhanced stability and reduced toxicity, ACS Appl. Nano Mater. 4 (9) (2021) 9213–9222, https://doi.org/10.1021/acsanm.1c01737.

[32] C. Zhang, Z. Wang, M. Wang, J. Shi, J. Wang, Z. Da, Y. Zhou, Y. Xu, N. V. Gaponenko, A.S. Bhatti, Ultrastable $CsPbBr_3$@$CsPb_2Br_5$@TiO_2 composites for photocatalytic and white light-emitting diodes, ACS Appl. Mater. Interfaces 15 (29) (2023) 35216–35226, https://doi.org/10.1021/acsami.3c07081.

[33] K. Du, L. He, S. Song, J. Feng, Y. Li, M. Zhang, H. Li, C. Li, H. Zhang, In situ embedding synthesis of highly stable $CsPbBr_3$/$CsPb_2Br_5$@PbBr(OH) nano/microspheres through water assisted strategy, Adv. Funct. Mater. 31 (36) (2021), https://doi.org/10.1002/adfm.202103275.

[34] G. Jiang, C. Guhrenz, A. Kirch, L. Sonntag, C. Bauer, X. Fan, J. Wang, S. Reineke, N. Gaponik, A. Eychmuller, Highly luminescent and water-resistant $CsPbBr_3$-$CsPb_2Br_5$ perovskite nanocrystals coordinated with partially hydrolyzed poly (methyl methacrylate) and polyethylenimine, ACS Nano 13 (9) (2019) 10386–10396, https://doi.org/10.1021/acsnano.9b04179.

[35] H. Zhang, M.-h. Shang, X. Zheng, Z. Zeng, R. Chen, Y. Zhang, J. Zhang, Y. Zhu, Ba^{2+} doped $CH_3NH_3PbI_3$ to tune the energy state and improve the performance of perovskite solar cells, Electrochim. Acta 254 (2017) 165–171, https://doi.org/10.1016/j.electacta.2017.09.091.

[36] C. Grote, B. Ehrlich, R.F. Berger, Tuning the near-gap electronic structure of tin-halide and lead-halide perovskites via changes in atomic layering, Phys. Rev. B 90 (20) (2014), https://doi.org/10.1103/PhysRevB.90.205202.

[37] D.B. Straus, R.J. Cava, Tuning the band gap in the halide perovskite $CsPbBr_3$ through Sr substitution, ACS Appl. Mater. Interfaces 14 (30) (2022) 34884–34890, https://doi.org/10.1021/acsami.2c09275.

[38] W. van der Stam, J.J. Geuchies, T. Altantzis, K.H. van den Bos, J.D. Meeldijk, S. Van Aert, S. Bals, D. Vanmaekelbergh, C. de Mello Donega, Highly emissive divalent-ion-doped colloidal $CsPb_{1-x}M_xBr_3$ perovskite nanocrystals through cation exchange, J. Am. Chem. Soc. 139 (11) (2017) 4087–4097, https://doi.org/10.1021/jacs.6b13079.

[39] J. Song, J. Li, X. Li, L. Xu, Y. Dong, H. Zeng, Quantum dot light-emitting diodes based on inorganic perovskite cesium lead halides ($CsPbX_3$), Adv Mater 27 (44) (2015) 7162–7167, https://doi.org/10.1002/adma.201502567.

[40] Y. Yu, Y. Liang, J. Yong, T. Li, M.S. Hossain, Y. Liu, Y. Hu, K. Ganesan, E. Skafidas, Low-temperature solution-processed transparent QLED using inorganic metal oxide carrier transport layers, Adv. Funct. Mater. 32 (3) (2021), https://doi.org/10.1002/adfm.202106387.

[41] Y. Dong, Y.K. Wang, F. Yuan, A. Johnston, Y. Liu, D. Ma, M.J. Choi, B. Chen, M. Chekini, S.W. Baek, L.K. Sagar, J. Fan, Y. Hou, M. Wu, S. Lee, B. Sun, S. Hoogland, R. Quintero-Bermudez, H. Ebe, P. Todorovic, F. Dinic, P. Li, H. T. Kung, M.I. Saidaminov, E. Kumacheva, E. Spiecker, L.S. Liao, O. Voznyy, Z. H. Lu, E.H. Sargent, Bipolar-shell resurfacing for blue LEDs based on strongly confined perovskite quantum dots, Nat. Nanotechnol. 15 (8) (2020) 668–674, https://doi.org/10.1038/s41565-020-0714-5.

[42] S. Chen, W. Cao, T. Liu, S.W. Tsang, Y. Yang, X. Yan, L. Qian, On the degradation mechanisms of quantum-dot light-emitting diodes, Nat. Commun. 10 (1) (2019) 765, https://doi.org/10.1038/s41467-019-08749-2.